JTE HCMUTE
ISSN: 2615-9740

JOURNAL OF TECHNICAL EDUCATION SCIENCE
Ho Chi Minh City University of Technology and Education
Website: https://jte.edu.vn
Email: jte@hcmute.edu.vn

Advanced Control Solution for Three-Phase Induction Motors in Magnetic Saturation Region

Vinh Quan Nguyen[1], Nhan Bon Nguyen[2], Thanh Lam Le*[2], Minh Tam Nguyen[2], Thuc Minh Bui[3]

[1]*Industrial University of Ho Chi Minh City, Vietnam*
[2]*Ho Chi Minh City University of Technology and Education, Vietnam*
[3]*Nha Trang University, Vietnam*

*Corresponding author. *Email: lamlethanh@hcmute.edu.vn*

ARTICLE INFO

Received: 08/01/2025
Revised: 28/01/2025
Accepted: 05/02/2025
Published online: 22/10/2025

KEYWORDS

Induction motor;
Torque control;
Robust control;
Magnetic saturation region;
Motor drives;
AC and DC drives.

ABSTRACT

In many industrial applications, induction motors are often required to operate in the magnetic saturation region to meet demands for high load or torque. However, in this region, the characteristics of the motor become nonlinear, rendering traditional control methods based on linear assumptions ineffective. This research focuses on the modeling and control of induction motors under magnetic saturation conditions. The motor model is developed in the d-q reference frame, incorporating nonlinear characteristics of both the stator and rotor. The study also introduces a signal modulation technique for a three-level inverter to enhance voltage conversion efficiency. To address the challenges posed by saturation effects and random disturbances, an enhanced direct torque control (EDTC) algorithm is proposed. This algorithm aims to mitigate the influence of magnetic saturation while maintaining robust performance. The proposed solution is validated through experimental testing conducted on the OPAL-RT system. Results confirm that the EDTC approach ensures the stator flux and speed closely track their reference values, even in the presence of noise. The control system delivers high performance, maintaining total harmonic distortion (THD) of the current within the range of 11% to 16%, underscoring its practicality and efficiency.

Doi: https://doi.org/10.54644/jte.2025.1760

1. Introduction

Induction motors are a cornerstone of modern engineering, widely used due to their robustness, simplicity, and cost-effectiveness [1], [2]. These motors are highly reliable, with minimal maintenance requirements, making them a preferred choice for a variety of applications in both industrial and domestic contexts. Their inherent ruggedness allows them to withstand harsh operating conditions, and they offer excellent durability and longevity compared to other motor types [3]-[5]. One of the significant advantages of induction motors is their flexibility in application. They are a key component in industrial systems, powering machinery such as pumps, compressors, and conveyors. Their use extends into transportation, where they drive electric trains and trams, and they play an increasingly pivotal role in electric and hybrid vehicles. Additionally, induction motors are integral to home appliances like refrigerators, washing machines, and air conditioners, underscoring their broad utility [6]-[8]. The popularity of induction motors in these domains is driven by several factors. They are highly energy-efficient, particularly when optimized with modern control systems such as vector control and predictive algorithms [9], [10]. These advancements allow for precise speed and torque control, enhancing performance in applications demanding dynamic operation. Moreover, the absence of brushes or permanent magnets simplifies their design, reducing initial and operational costs while eliminating the risk of magnet degradation [11].

Although three-phase induction motors are highly efficient, robust, and versatile in various applications, they are not without limitations, particularly under challenging operating conditions [12].

Magnetic saturation is a critical phenomenon that significantly impacts the performance and efficiency of these motors, especially during high load demands or transient scenarios such as startup or overload. When the magnetic core material of the motor approaches its flux-carrying capacity, its permeability diminishes, leading to a non-linear relationship between magnetic flux and current. This saturation effect results in elevated core losses, increased harmonic distortions, and a decline in overall efficiency [13]. Furthermore, the distortion in the magnetic field exacerbates thermal stress and mechanical vibrations, potentially shortening the motor's operational lifespan. Addressing these challenges requires the implementation of advanced strategies in motor design and control [14], [15].

Direct torque control (DTC) was independently developed by Isao Takahashi and Toshihiko Noguchi in 1986 [16], and officially introduced by Manfred Depenbrock in 1988 [17] as a control strategy called "Direct Self Control (DSC)," marking a revolutionary step in motor control technology. Since its inception, DTC has emerged as a prominent strategy for the efficient and precise operation of induction motors. Unlike traditional vector control methods, DTC offers a simpler structure by directly regulating the motor's torque and flux without the need for coordinate transformations or current controllers [18]. This approach ensures fast dynamic response and robust performance under various operating conditions. However, conventional DTC methods face challenges such as high torque and flux ripples, variable switching frequency, and sensitivity to parameter variations [19], [20], necessitating ongoing advancements to overcome these limitations.

Recent advancements in direct torque control aim to address its inherent limitations, with techniques like space vector modulation (DTC-SVM) playing a pivotal role in enhancing performance. DTC-SVM effectively maintains constant switching frequencies and reduces torque and flux ripples, significantly improving steady-state operation [21]-[23]. However, it also introduces certain challenges, including increased computational complexity and sensitivity to motor parameter variations, which can impact robustness and control accuracy. Furthermore, the implementation of DTC-SVM demands advanced hardware resources and real-time computational capabilities, making it less suitable for applications that prioritize fast and robust dynamic responses [24]. Furthermore, innovative methods such as duty-cycle control and model predictive torque control (MPTC) provide precise voltage vector selection, improving stability and performance across a wide range of speeds [25]. However, these methods are not without limitations. Duty-cycle control can struggle with increased complexity in calculating optimal duty ratios, while MPTC may face computational challenges due to the high burden of solving optimization problems in real-time [26], [27]. Additionally, integrating reinforcement learning and edge computing into DTC frameworks represents a groundbreaking advancement [28]. By utilizing data-driven optimization, these methods enable adaptive control strategies that address nonlinearities such as magnetic saturation and iron losses, ensuring robust and efficient motor operation. However, these approaches encounter several challenges, such as the computational complexity involved in training and inference, as well as safety risks associated with exploratory actions during the learning phase [29]. Furthermore, their reliance on high-quality training data and advanced hardware for real-time implementation can hinder their feasibility in cost-sensitive or resource-limited scenarios [30].

Controlling induction motors operating in the magnetic saturation region poses critical challenges, as traditional linear control models become inadequate due to inherent nonlinearities. By developing a comprehensive motor model in the d-q reference frame that accounts for saturation effects in both the stator and rotor, the research establishes a robust foundation for accurate dynamic analysis. To overcome the limitations posed by magnetic saturation and external disturbances, an enhanced direct torque control (EDTC) algorithm is introduced, incorporating an advanced signal modulation technique for three-level inverters to optimize voltage conversion efficiency. The effectiveness of the proposed method is rigorously validated through simulations and experimental testing using the OPAL-RT system. Results demonstrate the algorithm's ability to maintain precise control of stator flux and motor speed while ensuring low total harmonic distortion (THD) levels, even under challenging conditions. These findings underline the practicality and reliability of the approach, offering a significant contribution to the advancement of motor control strategies in industrial applications.

JTE
HCMUTE
ISSN: 2615-9740

JOURNAL OF TECHNICAL EDUCATION SCIENCE
Ho Chi Minh City University of Technology and Education
Website: https://jte.edu.vn
Email: jte@hcmute.edu.vn

2. Modeling and Control of Three-Phase Induction Motor

2.1. Induction motor modeling in the d-q reference frame

The modeling of induction motors in the d-q reference frame often assumes magnetic linearity for simplicity. However, in many applications requiring high torque, motors are forced to operate in the magnetic saturation region, where nonlinear characteristics become prominent. This section presents a nonlinear state-space model for induction motors under magnetic saturation, derived from the magnetic circuit representation of a rotor-stator tooth pair.

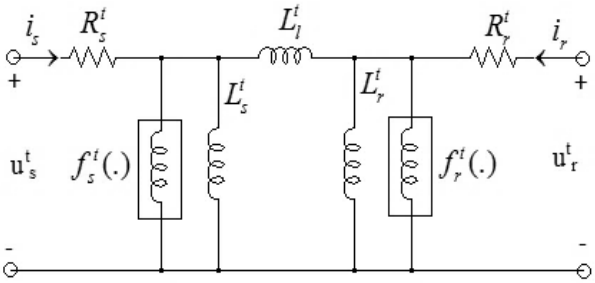

Figure 1. *Magnetic circuit model of an induction motor.*

Figure 1 illustrates the equivalent magnetic circuit model for a single rotor-stator tooth pair. In this model, the notation t denotes parameters specific to an individual tooth. Nonlinear quantities such as the mutual flux linkages $f_s^t(.)$, $f_r^t(.)$, and the inductances L_s^t, L_r^t, and L_l^t contribute to magnetic saturation in both the rotor and stator. The function $f(.)$ serves as a scalar mapping that defines the relationship between the magnitude of the input and the resulting output. Thus, the relationship between magnetic flux and current can be expressed mathematically as

$$\vec{\imath} = F(\vec{\varphi}) = \mathrm{f}(\|\vec{\varphi}\|)\frac{\vec{\varphi}}{\|\vec{\varphi}\|} \tag{1}$$

The inductance $\|\vec{\varphi}\|/f(\|\vec{\varphi}\|)$ is a nonlinear function of the magnetic flux magnitude $\|\vec{\varphi}\|$, where the current magnitude $\|\vec{\imath}\|$ is defined as $\|\vec{\imath}\| = \|\vec{\varphi}\| / \mathrm{L}(\|\vec{\varphi}\|)$. Two key nonlinear components, $F_s(.)$ and $F_r(.)$, are introduced to model the saturation effects. These functions describe the saturation behavior in the teeth of both the stator and rotor, incorporating only quadratic and higher-order terms to capture the nonlinearities effectively.

The electrical machine model integrates flux saturation effects in both the rotor and stator. Time derivatives are denoted using dot notation (.), reflecting the dynamic nature of the system. By leveraging the inherent symmetry of electrical machines, the resistance matrices R_s and R_r are constructed as scaled identity matrices, with the scalar resistance values representing the physical resistances. Subscripts s and r are used to distinguish stator-related and rotor-related parameters, respectively, including flux linkages (φ) and currents (i). These quantities are measured within the stationary reference frame for the stator and the rotor-aligned rotating reference frame for the rotor.

$$\begin{cases} \overrightarrow{i_s} = F_s(\overrightarrow{\varphi_s}) + \left(\dfrac{1}{L_s} + \dfrac{1}{L_1}\right)\overrightarrow{\varphi_s} - \dfrac{1}{L_1}\overrightarrow{\varphi_r} \\ \overrightarrow{i_r} = F_r(\overrightarrow{\varphi_r}) + \left(\dfrac{1}{L_r} + \dfrac{1}{L_1}\right)\overrightarrow{\varphi_r} - \dfrac{1}{L_1}\overrightarrow{\varphi_s} \\ \dot{\overrightarrow{\varphi_s}} = \overrightarrow{u_s} - R_s\overrightarrow{i_s} \\ \dot{\overrightarrow{\varphi_r}} = \overrightarrow{u_r} - R_r\overrightarrow{i_r} \end{cases} \tag{2}$$

If the reference frame is selected to align with the stator flux vector, the angular velocity of this coordinate system matches the rotational speed of the stator flux vector. In this configuration, the d-axis of the reference frame is aligned with the stator flux vector, simplifying the mathematical representation

JTE
HCMUTE
ISSN: 2615-9740

JOURNAL OF TECHNICAL EDUCATION SCIENCE
Ho Chi Minh City University of Technology and Education
Website: https://jte.edu.vn
Email: jte@hcmute.edu.vn

of the system dynamics. This choice ensures that the flux-oriented control strategy can be effectively implemented by maintaining a consistent relationship between the reference frame and the flux vector.

$$\begin{cases} \varphi_{sq} = \dot{\varphi}_{sq} = 0 \\ T_e = 1.5p\left(\varphi_{sd} i_{sq}\right) \\ \omega_r = \dfrac{u_{sq} - R_s i_{sq}}{\varphi_{sd}} = \dfrac{d\theta_m}{dt} \end{cases} \tag{3}$$

The dynamic equations governing the stator flux and current are fundamental to understanding the behavior of induction motors. These equations describe how the stator flux evolves over time under the influence of applied voltages and motor parameters, as well as how the stator current responds to changes in flux and rotor dynamics. These relationships are critical for developing control strategies that ensure precise torque and speed regulation in various operating conditions. By accurately modeling these dynamics, it becomes possible to predict and optimize motor performance, particularly in systems with nonlinear characteristics such as magnetic saturation.

$$\dot{\varphi}_{sd} = u_{sd} - R_s i_{sd} \tag{4}$$

$$i_{sq} = \frac{1}{L_l}\left[-\omega\varphi_{rd} + \frac{\varphi_{rd}}{\varphi_{sd}}\left(u_{sq} - R_s i_{sq}\right)\right] - R_r\left(\frac{1}{L_r} + \frac{1}{L_l}\right) i_{sq} - R_r \frac{f_r(\|\varphi_r\|)}{\|\varphi_r\|} i_{sq} \tag{5}$$

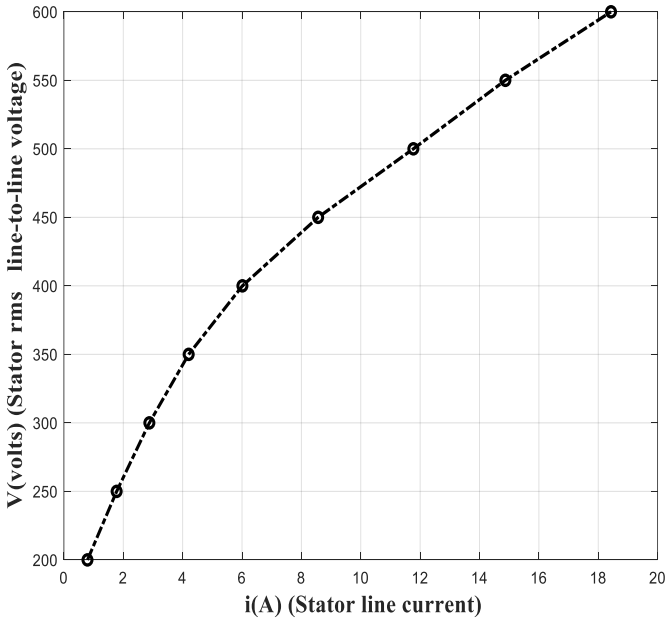

Figure 2. *Saturation characteristics of the motor.*

Figure 2 illustrates the no-load saturation characteristics of the motor, demonstrating the relationship between stator voltage and stator current under varying operating conditions. The stator voltage is varied from 200V to 600V, corresponding to stator current values ranging from 0.8A to 18A. The dashed line in the figure represents the motor's saturation parameters, highlighting the nonlinear relationship between the stator voltage and current. For the saturated motor, this nonlinear behavior is further depicted using the dotted curve, which aligns with the saturation parameters detailed in Table 1. This characterization provides essential insights into the motor's operational behavior in saturated conditions, forming the basis for advanced control strategies. The parameters presented in Figure 2 and Table 1 represent the characteristics of the motor used in the analysis and modeling of this study, serving as the basis for the experiments described in Section 3.

JTE
HCMUTE
ISSN: 2615-9740

JOURNAL OF TECHNICAL EDUCATION SCIENCE
Ho Chi Minh City University of Technology and Education
Website: https://jte.edu.vn
Email: jte@hcmute.edu.vn

Table 1. *Saturation parameters of the motor*

Saturation Parameters of the Motor (1HP - 400V - 150 rad/s)		**Measured Parameters (Unsaturated Motor)**	**Measured Parameters (Saturated Motor)**
V_{sat} (rms)	I_{sat} (peak A)	I_{sa} (peak A)	I_{sa} (peak A)
200	1.1232	1.1160	0.6450
250	2.5128	1.3950	1.1230
300	4.0712	1.6740	2.5080
350	5.9448	1.9530	4.0860
400	8.5039	2.2320	6.1090
450	12.1120	2.5110	8.6200
500	16.6480	2.7900	12.1800
550	21.0320	3.0690	16.5700
600	26.0640	3.3480	21.1700

2.2. Carrier-based modulation for three-level inverters

In this section, the three-level inverter is utilized to enhance voltage modulation precision and improve the overall efficiency of the induction motor control system. By offering a greater number of discrete voltage levels, this inverter topology significantly reduces harmonic distortion, resulting in smoother and more reliable motor operation compared to conventional two-level inverters. Moreover, the three-level inverter plays a crucial role in the EDTC strategy, facilitating accurate control of stator flux and torque, even in the presence of magnetic saturation. To achieve these advancements, the principles and implementation of carrier-based modulation for the three-level inverter are analyzed and discussed in the following section. Figure 3 illustrates the switching states of the cascaded three-level inverter for phase a, where S_{xj} represents the on-off state of the switches, with $x = a, b, c$.

$$Saj + S'aj = 1, j = 1,2 \tag{6}$$

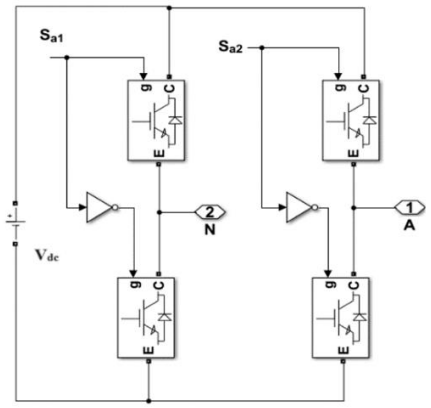

Figure 3. *Structure of the cascaded three-level inverter for a typical phase.*

Table 2. *Switching states for phase-a.*

n	$\boldsymbol{S_{a1}, S_{a2}}$	$\boldsymbol{Output\ voltage = (S_{a1} - S_{a2})V_{dc}}$
0	[0, 1]	$-V_{dc}$
1	[0, 0], [1, 1]	0
2	[1, 0]	V_{dc}

JTE
HCMUTE
ISSN: 2615-9740

JOURNAL OF TECHNICAL EDUCATION SCIENCE
Ho Chi Minh City University of Technology and Education
Website: https://jte.edu.vn
Email: jte@hcmute.edu.vn

For a three-level inverter ($n = 3$) with identical V_{dc} voltage sources, the corresponding switching states are presented in Table 2, allowing the output voltage to range continuously between $-V_{dc}$, 0, and $+V_{dc}$. Figure 4 illustrates the control model for the inverter, where $g(t)$ represents the control signal with an amplitude range of −1 to +1. This signal is adjusted to match the operating levels of the three-level inverter, producing the modified signal $G(t)$, which is defined by Equation (7). This adjustment ensures proper alignment with the inverter's switching logic and facilitates precise voltage modulation.

$$G(t) = [g(t) + 1]\frac{(n - 1)}{2} \tag{7}$$

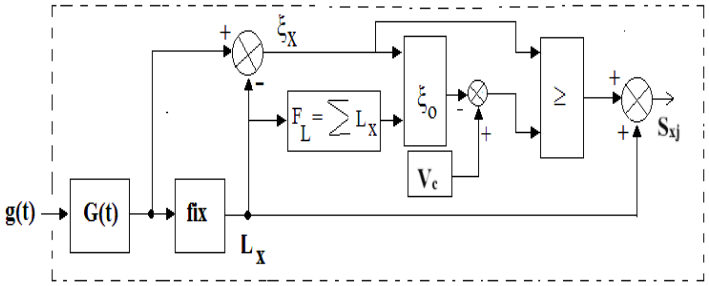

Figure 4. *Carrier-based modulation.*

The two components of the voltage G(t) are ξ_x and L_x, where $0 \le L_x \le n - 2$ represents the integer part of the $G(t)$ signal, defined by Equation (8)

$$L_x = \begin{cases} n - 2, & \text{if } G(t) \ge n - 2 \\ fix(G(t)), & \text{otherwise} \end{cases} \tag{8}$$

And $0 \le \xi_x \le 1$ represents the fractional part of the division, defined by

$$\xi_x = G(t) - L_x \tag{9}$$

Here, $n = 3$ denotes the number of levels in the inverter, V_c is the carrier wave for comparison, and S_{xj} refers to the switch states listed in Table 2.

The offset function ξ_o is proposed to be subtracted from the carrier wave, as illustrated in Figure 5. This adjustment ensures alignment with the inverter's modulation requirements and satisfies the condition defined by Equation (10). The total integer component, F_L, is expressed as the sum of L_x values across all three phases (x=a,b,c).

$$\xi_o = \begin{cases} 1\text{-max}(\xi_x), \text{ if } F_L = \frac{3(n-1)}{2} - 2 \\ -\text{min}(\xi_x), \text{ if } F_L = \frac{3(n-1)}{2} - 1 \\ 0, \text{ otherwise} \end{cases} \tag{10}$$

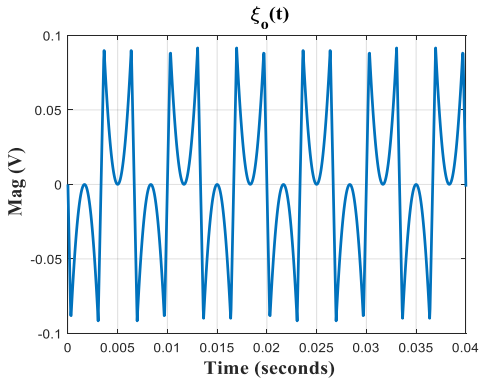

Figure 5. *Offset signal* $\xi_o(t)$.

2.3. Enhanced direct torque control

To enhance the performance of induction motors operating under magnetic saturation, a refined direct torque control strategy, referred to as enhanced direct torque control (EDTC), is proposed. Unlike conventional methods, this approach bypasses the challenges posed by the nonlinear components of magnetic saturation by leveraging measurable motor variables for direct control. By using u_{sd} to regulate stator flux ϕ_{sd} and u_{sq} to control current i_{sq}, the proposed control laws ensure independence from the saturation-induced nonlinearity. The following section outlines the derivation of these control equations, demonstrating how the method eliminates reliance on temperature-dependent parameters and ensures robust and efficient control under varying operating conditions. From Equations (4) and (5), it is observed that Equation (4) is entirely independent of magnetic saturation, whereas Equation (5) contains a nonlinear component, $fr(.)$, which accounts for the effects of saturation. However, since the current i_{sq} can be directly measured from the motor, it is utilized for control purposes, eliminating the need to rely on Equation (5). By assigning u_{sd} as the control variable for regulating φ_{sd} and u_{sq} as the control variable for i_{sq}, the control laws are formulated and expressed through the following equations

$$u_{\mathrm{sd}} = R_s i_{\mathrm{sd}} + K_{\varphi\mathrm{p}} e_{\varphi} + K_{\varphi\mathrm{i}} \int e_{\varphi} \mathrm{d}t \tag{11}$$

$$u_{\mathrm{sq}} = R_s i_{\mathrm{sq}} + K_{\mathrm{ip}} e_i + K_{\mathrm{ii}} \int e_i \, \mathrm{d}t \tag{12}$$

$$i^*_{\mathrm{sq}} = K_{\omega\mathrm{p}} e_{\omega} + K_{\omega\mathrm{i}} \int e_{\omega} \, \mathrm{d}t \tag{13}$$

The flux, torque, and speed errors are expressed as follows

$$e_{\varphi} = \varphi^*_{sd} - \varphi_{sd}, \; e_i = T^*_e - T_e, \; e_{\square} = \square^*_r - \square_r \tag{14}$$

Here, φ^*_{sd}, T^*_e, and ω^*_r are the reference values, while $K_{\varphi p}$, $K_{\varphi i}$, K_{ip}, K_{ii}, $K_{\omega p}$, and $K_{\omega i}$ are constants. The variables φ_{sd}, i_{sq}, and ω_r represent the measured values.

By substituting Equation (11) into Equation (4) and Equation (12) into Equation (5), the following results are obtained

$$\dot{\varphi}_{\mathrm{sd}} = K_{\varphi\mathrm{p}} e_{\varphi} + K_{\varphi\mathrm{i}} \int e_{\varphi} \mathrm{d}t \tag{15}$$

$$\omega_r = \frac{K_{\mathrm{ip}} e_i + K_{\mathrm{ii}} \int e_i \, \mathrm{d}t}{\varphi_{\mathrm{sd}}} \tag{16}$$

Next, by substituting Equation (15) into Equation (11) and Equation (16) into Equation (12), the resulting equations are derived as

$$u_{\mathrm{sd}} = R_s i_{\mathrm{sd}} + \dot{\varphi}_{\mathrm{sd}} \tag{17}$$

$$u_{\mathrm{sq}} = R_s i_{\mathrm{sq}} + \varphi_{\mathrm{sd}} \omega_r \tag{18}$$

$$\varphi_{\mathrm{sd}} = \int \dot{\varphi}_{\mathrm{sd}} \mathrm{d}t \tag{19}$$

$$\theta_m = \int \omega_r \mathrm{d}t \tag{20}$$

It is observed that Equations (15), (16), (19), and (20) are independent of magnetic saturation, and the term $R_s i_{sq}$ does not appear. Consequently, the stator flux and the angular position θ_m are unaffected

by variations in R_s, even under changing temperature conditions. Specifically, Equations (15) and (19) estimate the stator flux φ_{sd}, while Equation (3) provides an estimation for the electromagnetic torque T_e. The angular position θ_m is determined using Equation (20), and the voltages u_{sd} and u_{sq} are calculated from the pair of Equations (17) and (18).

3. Analysis and Discussion

In this section, experiments are conducted to validate the proposed approach. The system under test consists of a three-phase squirrel cage induction motor, with its parameters specified in Table 3. A cascaded three-level inverter with a carrier frequency of $V_c = 1.5\,kHz$ is utilized for performance evaluation. The OPAL-RT platform is employed to execute the control algorithms for the three-phase induction motor system. The motor speed is measured through feedback provided by an encoder with a resolution of 1024 pulses per revolution. Figure 6 presents the general block diagram of the EDTC algorithm for a three-phase induction motor. The speed and flux controllers generate reference signals, which are processed by the torque controller and dq-to-abc transformation to produce control inputs for the IGBT inverter. Operating in a closed-loop configuration, the system continuously adjusts based on measured current and speed feedback, ensuring precise torque and flux regulation under varying load conditions. In this setup, torque and flux are independently controlled, while the speed is managed indirectly. The experimental configuration of the system is shown in Figure 7.

Table 3. *System parameters*

Power	1 (Hp)
Voltage (line-line)	400 (V)
R_s, L_s	2.5 (Ω), 5(mH)
R_r, L_r	0.816 (Ω), 5(mH)
ω_r	150 (rad/s)
T_e	5 (N.m)
f_c	1.5 (kHz)
Dead time	2.5 (µs)
p	2
J	0.005 (kg.m2)
L_m	50.31(mH)
T_s	40 (µs)
V_{dc}	200 (V)

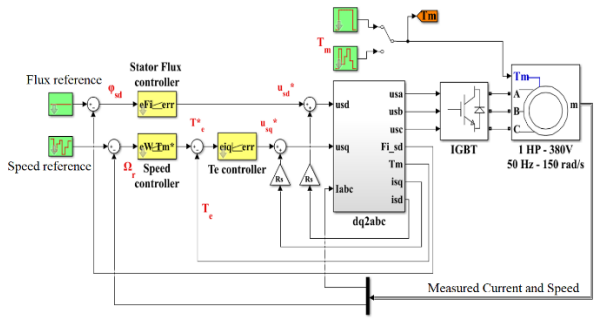

Figure 6. *Block Diagram of the EDTC for the three-phase induction motor system.*

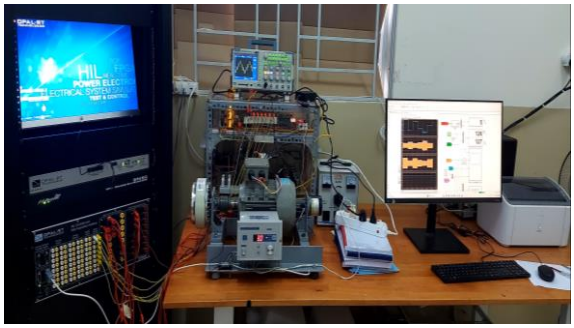

Figure 7. *Experimental setup.*

JTE
HCMUTE
ISSN: 2615-9740

JOURNAL OF TECHNICAL EDUCATION SCIENCE
Ho Chi Minh City University of Technology and Education
Website: https://jte.edu.vn
Email: jte@hcmute.edu.vn

The results of the output quality analysis for the three-level inverter are presented in Figure 8. The line-to-line voltage (V_{ab}) between two phases was measured and subjected to FFT analysis to evaluate its harmonic content. Additionally, the common-mode voltage (CMV) was measured and visually displayed. Figure 8 illustrates the experimental results for V_{ab}, CMV, and the THD spectrum of the line voltage, conducted under conditions of $T_m = 5$ Nm and a reference speed $\omega_r^* = 150$ rad/s. The results indicate that the inverter outputs are stable and of high quality. Furthermore, the findings demonstrate that the motor's flux and speed closely track their reference values. Figure 9a shows the experimental results for $T_m = 5$ Nm, where the reference flux (blue line) and the measured flux (red dashed line) reach steady-state within approximately 0.75 seconds. Figure 9b presents the measured speed (red dashed line) and the reference speed (blue line), achieving steady-state within approximately 1.0 second.

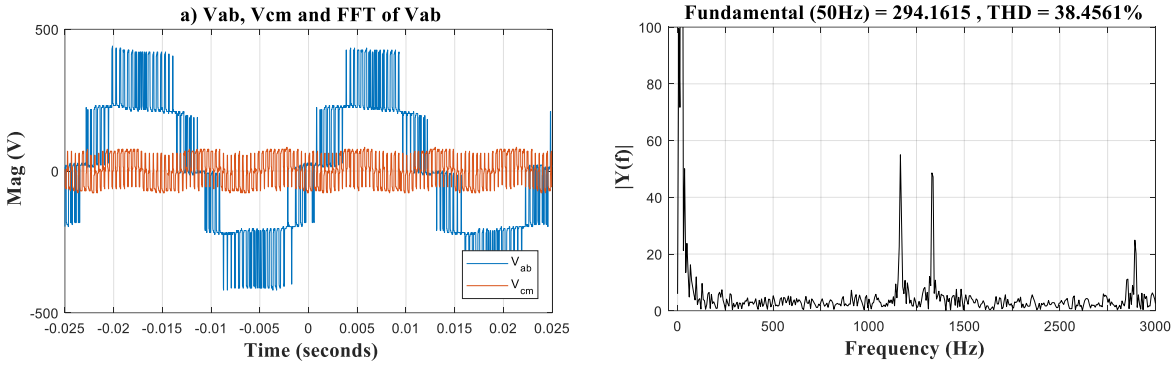

(a) (b)

Figure 8. *Experimental results for $T_m = 5$ Nm and $\omega_r^* = 150$ rad/s. a) V_{ab} and V_{cm}, b) FFT of V_{ab}.*

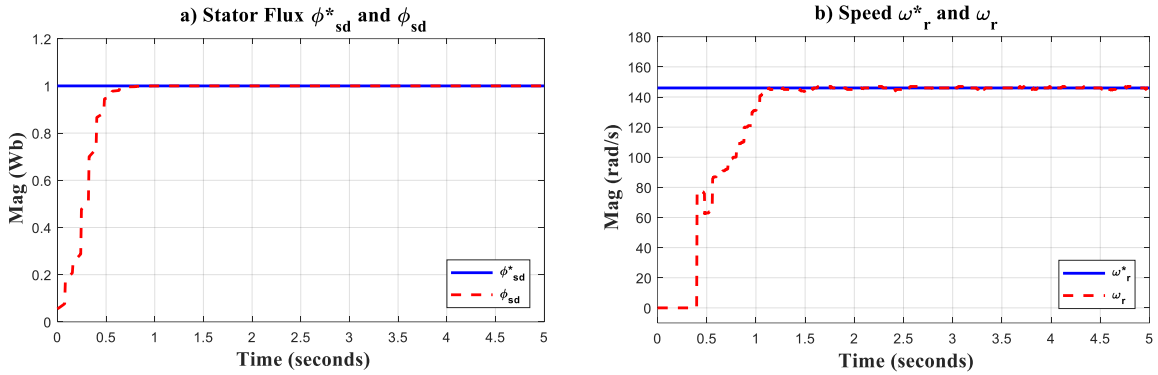

Figure 9. *Experimental results of flux and speed response. a) Flux, b) Speed.*

An investigation was conducted with a torque of 5 Nm while varying the motor speed. Figure 10 illustrates that the measured flux aligns closely with the reference flux. Additionally, the measured speed tracks the reference speed effectively across the range of speed variations, from 3 rad/s to 30 rad/s. Figure 10b shows that the stator current in phase a reaches approximately 2.5 A at speeds of 3 rad/s and 30 rad/s, with a THD of 11%. The study also examined the system's performance under the influence of noise. Figure 11a presents the experimental results when subjected to a noise signal $d(t)$, indicating that the flux and speed continue to follow their reference values effectively. However, at speeds of 3 rad/s and 30 rad/s, the measured speed exhibits significant oscillations around the reference values. Figure 11b reveals that the stator current in phase a increases to approximately 3 A under these conditions, with the current THD rising to 16%.

The validation performed on the OPAL-RT platform demonstrates the effectiveness and high performance of the proposed control solution, particularly for the direct control of flux and torque. The control system remains robust and stable, even when the motor speed varies significantly from a maximum of 150 rad/s to a minimum of 3 rad/s, while also enduring the presence of external disturbances. This study focuses on induction motors operating under magnetic saturation, a condition

JTE
HCMUTE
ISSN: 2615-9740

JOURNAL OF TECHNICAL EDUCATION SCIENCE
Ho Chi Minh City University of Technology and Education
Website: https://jte.edu.vn
Email: jte@hcmute.edu.vn

where nonlinearity naturally elevates THD. In industrial applications, such levels are often acceptable as a trade-off for achieving robust torque and flux control. Notably, similar studies frequently report THD values within the 10%-20% range, consistent with our findings. Importantly, reducing THD is not the primary objective of this research; rather, the emphasis is on ensuring control stability and efficiency under demanding conditions. These results underscore the system's resilience to dynamic operating scenarios and external disturbances, affirming its suitability for industrial applications where motors operate in challenging environments.

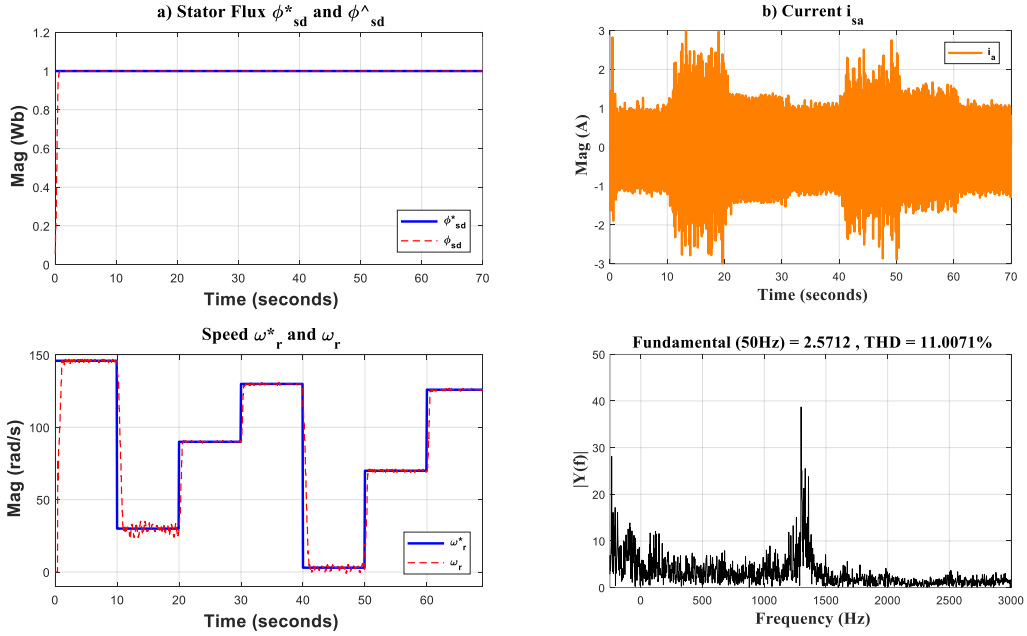

Figure 10. *Experimental results for torque 5 Nm and varying motor speed. a) Flux and speed; b) Phase current and FFT of phase current.*

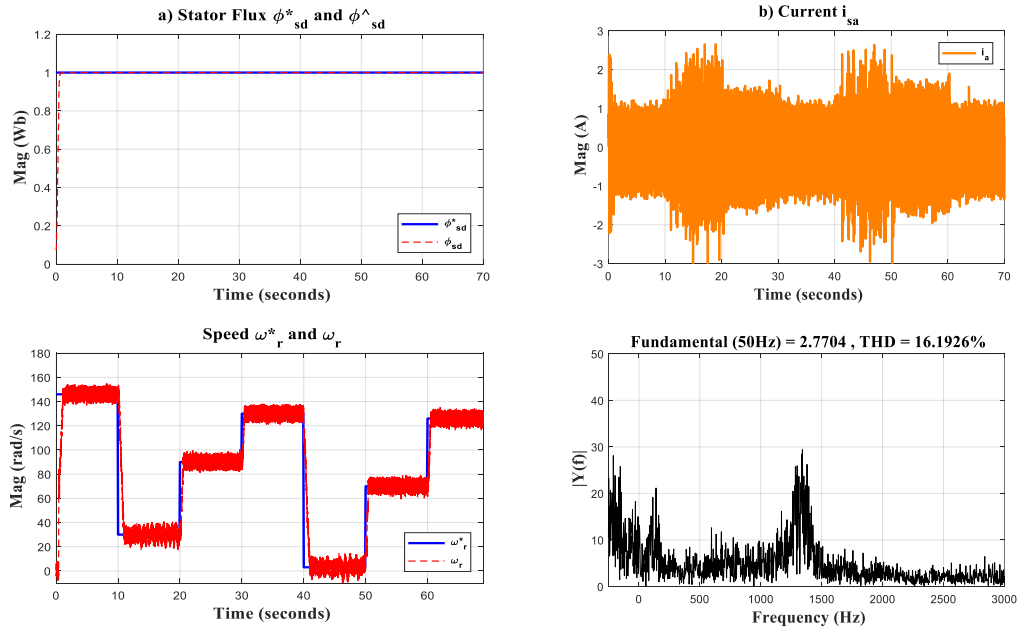

Figure 11. *Experimental results with d(t). a) Flux and speed; b) Phase current and FFT of phase current.*

4. Conclusion

This study addresses the significant challenges in controlling three-phase induction motors operating in the magnetic saturation region. By developing a nonlinear motor model in the d-q reference frame and incorporating advanced techniques such as carrier-based modulation for three-level inverters, the research presents a robust solution to enhance voltage modulation accuracy and overall control efficiency. The EDTC algorithm was proposed to mitigate the effects of magnetic saturation and external disturbances. Experimental validation conducted on the OPAL-RT platform demonstrated the system's ability to maintain precise flux and torque control while ensuring stability and reliability under varying speed and noise conditions. The findings underline the robustness and practical applicability of the proposed control strategy, offering a significant contribution to the development of motor control solutions suitable for industrial environments demanding high performance and efficiency. Future work will explore potential methods to reduce THD, such as optimizing the control algorithm, implementing harmonic filters, and refining the modulation strategy to enhance system performance.

Conflict of interest

The authors declare no conflicts of interest.

REFERENCES

[1] W. Qiu, X. Zhao, A. Tyrrell, S. Perinpanayagam, S. Niu, and G. Wen, "Application of artificial intelligence-based technique in electric motors: A review," *IEEE Transactions on Power Electronics*, vol. 39, no. 10, pp. 13543–13568, Oct. 2024.

[2] M. Popescu, L. D. Leonardo, G. Fabri, G. Volpe, N. Riviere, and M. Villani, "Design of induction motors with flat wires and copper rotor for E-vehicles traction system," *IEEE Transactions on Industry Applications*, vol. 59, no. 3, pp. 3889–3900, May–June 2023.

[3] L. Wogi, A. Thelkar, T. Tahiro, T. Ayana, S. Urooj, and S. Larguech, "Particle swarm optimization based optimal design of six-phase induction motor for electric propulsion of submarines," *Energies*, vol. 15, no. 9, p. 2994, Apr. 2022.

[4] A. Kasri, K. Ouari, Y. Belkhier, M. Bajaj, and I. Zaitsev, "Optimizing electric vehicle powertrains peak performance with robust predictive direct torque control of induction motors: A practical approach and experimental validation," *Scientific Reports*, vol. 14, no. 14977, Jun. 2024.

[5] Q. N. Vinh and T. L. Le, "Optimal frequency modulation of carrier waves and its application to induction motor drive systems," *Electrical Engineering*, Dec. 2024.

[6] H. V. Coutinho, J. A. Toledo, L. A. R. Silva, and T. A. C. Maia, "Design and implementation of a low-cost and low-power converter to drive a single-phase motor," *Machines*, vol. 11, no. 7, p. 673, Jun. 2023.

[7] A. N. Abdullah, A. H. Mutlag, and M. S. Ahmed, "Neural network based home energy management for modelling and controlling home appliances under demand response," *Journal of Physics: Conference Series*, vol. 1963, no. 1, p. 012097, May 2021.

[8] S. Ghosh, A. Chatterjee, and D. Chatterjee, "An improved load feature extraction technique for smart homes using fuzzy-based NILM," *IEEE Transactions on Instrumentation and Measurement*, vol. 70, article no. 2511209, Jul. 2021.

[9] T. L. Le, M. F. Hsieh, and M. T. Nguyen, "Robust speed control with disturbance rejection for surface-mounted permanent magnet synchronous motor," *Proc. 6th Int. Conf. Green Technol. Sustain. Dev. (GTSD)*, pp. 459–463, Jul. 2022.

[10] M. Affan and R. Uddin, "Brain emotional learning and adaptive model predictive controller for induction motor drive: A new cascaded vector control topology," *International Journal of Control, Automation and Systems*, vol. 19, pp. 3122–3135, 2021.

[11] R. R. Kumar, M. Andriollo, G. Cirrincione, M. Cirrincione, and A. Tortella, "A comprehensive review of conventional and intelligence-based approaches for the fault diagnosis and condition monitoring of induction motors," *Energies*, vol. 15, no. 23, p. 8938, Nov. 2022.

[12] M. A. Sheikh, S. T. Bakhsh, and M. Irfan, "A review to diagnose faults related to three-phase industrial induction motors," *Journal of Failure Analysis and Prevention*, vol. 22, pp. 1546–1557, Jul. 2022.

[13] R. Kumar and P. Kumar, "Core loss estimation for an inverter-fed induction motor with more accurate realisation of material non-linearity and impact of hysteresis minor loops," *IEEE Transactions on Energy Conversion*, vol. 37, no. 1, pp. 327–336, Mar. 2022.

[14] M. F. Hsieh, Y. H. Chang, and D. G. Dorrell, "Design and analysis of brushless doubly fed reluctance machine for renewable energy applications," *IEEE Transactions on Magnetics*, vol. 52, no. 7, article no. 8204705, Jul. 2016.

[15] P. D. Nguyen, A. V. Vo, T. L. Le, and G. T. T. Lai, "Field-oriented control strategy for induction motor drives," *Eastern International University Scientific Conference 2023 (EIUSC 2023)*, pp. 438–445, Nov. 2023.

[16] I. Takahashi and T. Noguchi, "A new quick-response and high-efficiency control strategy of an induction motor," *IEEE Transactions on Industry Applications*, vol. IA-22, no. 5, pp. 820–827, 1986.

[17] M. Depenbrock, "Direct self-control (DSC) of inverter-fed induction machine," *IEEE Transactions on Power Electronics*, vol. 3, no. 4, pp. 420–429, Oct. 1988.

[18] J. Cai, X. Dou, A. D. Cheok, Y. Yan, and X. Zhang, "Overview of the direct torque control strategy in switched reluctance motor drives," *IEEE Transactions on Transportation Electrification*, Early Access, pp. 1–1, Jun. 2024.

[19] T. L. Le and M. F. Hsieh, "An enhanced direct torque control strategy with composite controller for permanent magnet synchronous motor," *Asian Journal of Control*, vol. 26, no. 4, pp. 1683–1702, Jul. 2024.

[20] S. S. Sivaraju, T. Senthilkumar, R. Sankar, T. Anuradha, S. Usha, and I. B. Musirin, "Improving the efficiency of induction motor drive by flux and torque control: A hybrid LSE-RERNN approach," *ISA Transactions*, vol. 147, pp. 215–226, Apr. 2024.

[21] S. Savarapu, M. Qutubuddin, and Y. Narri, "Modified brain emotional controller-based ripple minimization for SVM-DTC of sensorless induction motor drive," *IEEE Access*, vol. 10, pp. 40872–40887, Apr. 2022.

[22] F. Z. Latrech, A. B. Rhouma, and A. Khedher, "FPGA implementation of a robust DTC-SVM based sliding mode flux observer for a double star induction motor: Hardware in the loop validation," *Microelectronics Reliability*, vol. 150, p. 115118, Nov. 2023.

[23] F. B. Salem, M. T. Almousa, and N. Derbel, "Enhanced control technique for induction motor drives in electric vehicles: A fractional-order sliding mode approach with DTC-SVM," *Energies*, vol. 17, no. 17, p. 4340, Aug. 2024.

[24] N. K. Shukla, R. Srivastava, and S. Mirjalili, "A hybrid dragonfly algorithm for efficiency optimization of induction motors," *Sensors*, vol. 22, no. 7, p. 2594, Mar. 2022.
[25] Y. Zhang and H. Yang, "Model predictive torque control of induction motor drives with optimal duty cycle control," *IEEE Transactions on Power Electronics*, vol. 29, no. 12, pp. 6593–6603, Dec. 2014.
[26] C. Zhang, B. Xu, J. Jasni, M. A. M. Radzi, N. Azis, and Q. Zhang, "Three voltage vector duty cycle optimization strategy of the permanent magnet synchronous motor driving system for new energy electric vehicles based on finite set model predictive control," *Energies*, vol. 16, no. 6, p. 2684, Mar. 2023.
[27] S. Gao, Y. Wei, D. Zhang, H. Qi, and Y. Wei, "A modified model predictive torque control with parameters robustness improvement for PMSM of electric vehicles," *Actuators*, vol. 10, no. 6, p. 132, Jun. 2021.
[28] S. Zhang, O. Wallscheid, and M. Porrmann, "Machine learning for the control and monitoring of electric machine drives: Advances and trends," *IEEE Open Journal of Industry Applications*, vol. 4, pp. 188–214, Jun. 2023.
[29] A. Farea, O. Y. Harja, and F. E. Streib, "Understanding physics-informed neural networks: Techniques, applications, trends, and challenges," *AI*, vol. 5, no. 3, pp. 1534–1557, Aug. 2024.
[30] A. S. Chivukula, X. Yang, B. Liu, W. Liu, and W. Zhou, "Game theoretical adversarial deep learning," in *Adversarial Machine Learning*, Springer, Cham, 2023.

Vinh Quan Nguyen received the M.S. degree in automation technology from HCM City University of Technology (HCMUT), Vietnam, and the Ph.D. degree in electrical engineering from HCMUT, Vietnam. He is currently a lecturer in the Faculty of Electronics Technology, Industrial University of Ho Chi Minh City, Vietnam. His research interests are circuit design, and power electronics.
He can be reached via email at quan_01037027@iuh.edu.vn. ORCID: https://orcid.org/0009-0007-3756-882X

Nhan Bon Nguyen is a former student of HCM City University of Technology, Vietnam, where he earned his Ph.D. in electrical engineering. He is currently a lecturer in the Faculty of Electrical and Electronics Engineering at HCM City University of Technology and Education. His research interests include power systems, transmission grid troubleshooting, and optimization algorithms.
He can be reached via email at bonnn@hcmute.edu.vn. ORCID: https://orcid.org/0000-0001-9007-5302

Thanh Lam Le received the M.S. degree in electrical engineering from HCM City University of Technology, Vietnam, and the Ph.D. degree in electrical engineering from National Cheng Kung University, Tainan, Taiwan. He is currently a lecturer in the Faculty of Electrical and Electronics Engineering, Ho Chi Minh City University of Technology and Education (HCMUTE). His research interests include motor drives, energy conversion systems, advanced control theory and its applications.
He can be reached via email at lamlethanh@hcmute.edu.vn. ORCID: https://orcid.org/0009-0008-8562-2031

Minh Tam Nguyen received his M.S. degree in Electrical Engineering from Ho Chi Minh City University of Technology, Vietnam and his Ph.D. degree in Engineering Science from the University of Technology, Sydney, Australia. He is currently a lecturer in the Control Engineering and Automation Department, Faculty of Electrical and Electronics Engineering at Ho Chi Minh City University of Technology and Education (HCMUTE), Vietnam. His research interests include system modeling, intelligent and robust control, and soft computing.
He can be reached via email at tamnm@hcmute.edu.vn. ORCID: https://orcid.org/0009-0000-8230-1373.

Thuc Minh Bui received his M.S. degrees in Electrical Engineering from Ho Chi Minh City University of Technology and Educcation, and his Ph.D. degree in electrical engineering at from Yeungnam University in Gyeongsan, Korea. He is currently a lecturer at the Faculty of Electrical and Electronics Engineering at Nha Trang University in Nha Trang City, Vietnam. His research interests include control theory, power converter, automation, and optical science with applications to industry and the environment.
He can be reached via email at minhbt@ntu.edu.vn. ORCID: https://orcid.org/0000-0001-9208-6873.